Title

Quasi-3-D Dynamic Model of an Internally Reforming Planar Solid Oxide Fuel Cell for Hydrogen Co-Production

ISBN

978-0-7918-4318-5

Authors

Shaffer, Brendan
Hunsuck, Michael
Brouwer, Jacob

Publication Date

2008

DOI

10.1115/fuelcell2008-65193

Proceedings of FuelCell2008
Sixth International Fuel Cell Science, Engineering and Technology Conference
June 16-18, 2008, Denver, Colorado, USA

FuelCell2008-65193

QUASI-3-D DYNAMIC MODEL OF AN INTERNALLY REFORMING PLANAR SOLID OXIDE FUEL CELL FOR HYDROGEN CO-PRODUCTION

Brendan Shaffer, Michael Hunsuck and Jacob Brouwer*

National Fuel Cell Research Center
University of California, Irvine, California, 92697-3550
***corresponding author: jb@nfcrc.uci.edu; tel: 949-824-1999; fax: 949-824-7423**

ABSTRACT

A simplified quasi-3-dimensional model of a solid oxide fuel cell (SOFC) is developed to investigate the dynamics of internal reformation in an SOFC. The dynamic model solves dynamic equations that govern relevant physical and chemical processes in a simplified geometric representation of a planar SOFC. This makes the model complex enough to resolve major performance characteristics and simple enough to be used in dynamic analyses and controls development at the system level. The model solves dynamic mass, momentum and energy conservation equations to provide local temperature, species concentrations, and current density distributions. These distributions are resolved in two dimensions across the cell, but each 2-D distribution resolves 5 separate control volumes through the nodal unit cell: the PEN; anode and cathode gas compartments; and interconnects. Internal reforming chemical kinetic expressions are included in the model formulation. Simulations show that extent of internal reformation impacts the dynamic temperature difference across the cell. Steady state maximum temperature differential across the cell can be reduced to about 100 K with 100% internal reformation and a cross-flow configuration. A full hydrogen co-production system was then modeled by integrating the SOFC model with heat exchangers, combustor, blower, and hydrogen collector. For conditions of a constant cathode exhaust temperature of 1273 K and lower fuel utilization (60% - 70%), the dominant thermal influence on the cell temperature was cooling by the endothermic reformation reactions. But at higher fuel utilization conditions, the dominant thermal influence was the convective cooling of the cathode gases. System simulations showed no tradeoff between power and H_2 production if the cathode exhaust temperature is held constant at 1273 K. High power and high H_2 production conditions were found to be synergistic: high hydrogen production leads to high electrochemical efficiency and lower air flow rate leading to fewer parasitic losses. Dynamic SOFC responses to manipulation of fuel flow rate within the range of fuel utilization between 60 and 85% indicate that the system can be adequately controlled to produce various amounts of hydrogen and electricity.

INTRODUCTION

The scenario of the “hydrogen economy” is often looked upon as an energy utopia. Solar, wind, and hydro energy sources would be used to convert water to hydrogen through electrolysis that could then be used in most portable, automotive, and industrial applications. This scenario is perceived as being one of the most favorable states for energy transmission and conversion.

But there are significant hurdles associated with implementing a hydrogen economy. One of these hurdles is the current lack of any significant infrastructure to produce, store, transport, and distribute hydrogen [1]. But alas, as long as current energy carriers and infrastructure are cheaper than building a new infrastructure, and as long as concomitant environmental damage is tolerated by the general public, there will never be sufficient impetus to build hydrogen infrastructure without hydrogen demand already in place.

The proton exchange membrane fuel cell (PEMFC) is typically associated with the hydrogen economy, due to its need for and efficient use of pure hydrogen to produce electricity. Solid oxide fuel cells (SOFCs), on the other hand, are more directly applicable to current infrastructure fuels, such as natural gas. The current work explores an application in which SOFC technology could become a catalyst for bringing about a hydrogen economy. Unlike most other fuel cells, SOFCs possess the unique ability to operate not only on pure hydrogen

but also on reformate of natural gas and in some cases on natural gas directly. In this way, fuel cells can be introduced into current commercial and industrial sectors while running on a common fuel. It is hoped that public and commercial acceptance of SOFCs would facilitate the emergence of hydrogen- fuel cells as well.

If a hydrogen economy were to come about, one novel capability of SOFCs (and other high temperature fuel cells) is their ability to co-produce hydrogen fuel along with generating electricity. This concept is often referred to as "hydrogen co-production." The key to this concept of hydrogen co-production is based upon a symbiotic relationship between natural gas reforming processes and fuel cell electrochemical processes. The reformer needs heat and the fuel cell needs to rid itself of heat. This transfer of heat could be done with minimal losses if it could be done inside the fuel cell itself. First, the energy conversion efficiency will theoretically be higher [2]. Second, less air will be needed for cooling, so the air flow rate can be decreased resulting in fewer parasitic losses from an air compressor [3].

However, there are also potential disadvantages to on-anode fuel reformation. These potential disadvantages include the possibility of large temperature gradients in the fuel cell as well as the possibility of "coking," which is the condition where carbon is formed and deposited on the electrode causing blockage and slowing of reactions [3,4]. The problem posed by internal reformation leading to large temperature gradients is is investigated in this paper. The problem of coking is left as a topic of future research. It should be noted that the current effort limits the range of internal reforming investigation to higher temperatures (greater than 1273 K) and a steam-to-carbon (SC) ratios of 3 where coking is known to be less of a problem [5,6].

Despite the ample literature on the modeling of SOFCs, a smaller population of literature with regard to the dynamic modeling of SOFCs exists. One of the early dynamic models was Achenbach's [7], which is probably the most referenced SOFC model in the literature [8]. Other dynamic models include those presented in [9-17]. Of these models four are planar SOFC dynamic models [7, 9-11]. However, only Achenbach's model gives 3-D resolution, but Achenbach's model could not be used as part of a larger system simulation because of the computational time required. The ecurrent model development approach is desired for its ability to be used in a larger system simulation without the loss of pertinent spatially-resolved (2-D) information, such as the temperature distribution across the PEN or separator plate. This also allows the current model to be used in the development of control strategies for system implementation.

The current SOFC model was used to investigate the dynamics of internal reformation in an SOFC both as an isolated fuel cell and as a part of a larger system. This integration into a larger system demonstrates how the model can be integrated into larger system simulations. The larger system consists of a heat exchanger, blower, combustor, and a hydrogen collector in addition to the fuel cell. The SOFC model was used to perform steady state as well as dynamic simulations. The steady state simulations were used to examine the effects of pre-reforming, including no pre-reforming, partial pre-reforming, and complete pre-reforming. Steady state simulations using the hydrogen co-production system model were also done in order to analyze the performance of such a system. The SOFC model was then used to simulate the dynamics of the SOFC associated with changes in the fuel utilization. For these dynamic simulations the fuel cell was not integrated into the larger system model.

MODEL

Fuel cell

Since the fuel cell model is the main component in the system and the focus of this paper, considerable detail is provided here to explain the assumptions used and the equations that are solved in order to obtain the results in this paper.

Assumptions

The fuel cell and system components are modeled using MATLAB Simulink®. Most of the assumptions used for the model are the same as those used by Mueller et al. [18], which include but are not limited to the following:

(1) The flow in the fuel cell is laminar.
(2) The fuel cell is well insulated, so there are no heat losses.
(3) The electrodes are made of highly conductive material so that they are an equipotential surface.
(4) The fuel cell is discretized into 16 fuel cell "nodes" which are control volumes that are characterized by a lumped temperature and lumped species concentrations.
(5) Pressure drops in the fuel cell are negligible.
(6) Radiation heat transfer is negligible since convective and conductive heat transfer dominate.
(7) Conduction along the PEN is negligible since it is a thin ceramic.
(8) Coking is negligible. Note: Previous research suggests this should be a good assumption for high SC ratios, but if further research is done in this area it should definitely take the effects of coking into account.
(9) The gases are ideal and incompressible, but not calorically perfect.
(10) The electrochemistry is rapid so that the electrochemical reactions are directly proportional to the current.
(11) The CH_4 and CO are not oxidized directly but are reformed and shifted to H_2 which is then electrochemically reacted.
(12) The fuel reformation takes place in two steps. First, CH_4 is reformed to CO and H_2. Then the CO is

converted to H_2 via the water-gas shift reaction. The kinetics of the reformation reactions are outlined by Achenbach and Riensche [19]. The reformation of CH_4 to CO is described by an Arrhenius expression and the water-gas shift reaction is assumed to reach equilibrium almost immediately.

Fuel Cell Stack

The fuel cell stack consists of individual cells stacked and electrically connected in series to achieve a desired voltage and power output. The individual cells are stacked in series so as to have the same current and be additive in voltage. Then these stacks are connected in parallel so that they have the same voltage and are additive in current. The entire fuel cell is modeled using only a single cell which is assumed to be representative of the rest, and then the power and voltage for the entire collection of cells is determined by the appropriate multiplication factors according to how many cells are in series and how many stacks are in parallel in the system.

Cell Discretization

In order to determine the temperature and species concentration gradients within the representative cell, the cell is discretized into a number of control volumes, which will be referred to as "nodes." Sixteen nodes are used in the analysis. Each node is subject to species and energy balances, and thus the properties of the node as well as the flow properties into and out of the node can be determined by dynamically solving the conservation equations simultaneously.

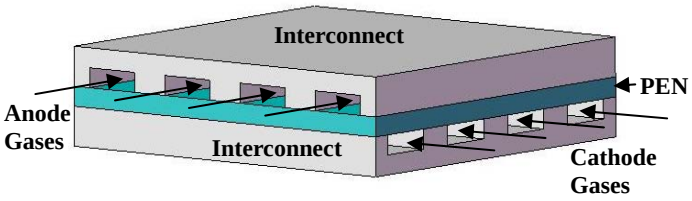

Figure 1. Schematic of a solid oxide fuel cell.

The cell is set up in a cross flow configuration as shown in Figure 1. The anode and cathode gases flow into and out of adjacent sides of the stack. For the purpose of consistent plotting of simulation results, the anode gases are always taken as flowing from left to right and the cathode gases are taken as flowing from front to back.

Electrochemical Reactions

At every node, there are two different types of reactions taking place, chemical reactions and electrochemical reactions. The chemical reactions govern the reformation of CH_4 while H_2 reacts electrochemically. However, both the cathode and the anode experience electrochemical reactions, which are split into two half-reactions. The oxidation half-reaction occurs at the anode and the reduction half-reaction occurs at the cathode.

The electrochemical reactions included are shown below. The first half-reaction occurs at the anode and the second occurs at the cathode.

$$H_2 + O^{2-} \rightarrow 2e^- + H_2O \quad (1)$$

$$\tfrac{1}{2}O_2 + 2e^- \rightarrow O^{2-} \quad (2)$$

The electrochemical half reactions are assumed to produce their ideal number of electrons. This results in the rate of reaction for the electrochemical reactions being:

$$R = \pm\frac{i}{nF} \quad (3)$$

For H_2, the sign is negative since H_2 is being consumed, and the value for *n* is two since there are two moles of electrons produced for every mole of H_2 consumed. Likewise, the sign for H_2O is positive with an *n* value of two, and the sign for O_2 is negative with an *n* value of four.

The electrochemical reactions are exothermic, so in order to prevent the cell from overheating, this heat must be transferred to the anode and cathode gas streams, lost to the environment, or consumed bythe endothermic reformation reactions.

Reformation Reactions

Since this paper investigates the reformation of CH_4 directly on the anode, the kinetics of the two reformation reactions are of utmost importance. The first of these two reactions is the methane reformation reaction, which describes CH_4 and steam being reformed to CO and H_2 in a nickel yttria-stabilized-zirconia (Ni-YSZ) anode.

$$CH_4 + H_2O \rightarrow CO + 3H_2 \quad (4)$$

The second reaction is the water-gas shift reaction. It takes the CO produced in the first reaction along with more steam and produces CO_2 and more H_2.

$$CO + H_2O \rightarrow CO_2 + H_2 \quad (5)$$

Both of these reactions are reversible, but tend to proceed fairly quickly in the forward direction when methane and steam are introduced to the anode compartment. Typical SOFC operating temperatures and nickel-yttria-stabilized zirconia anodes produce conditions that often deplete the CH_4 before getting very far into the cell. The methane reformation reaction of equation (4) is typically rate-limiting.

Aguiar et al. [21] reviewed a wide range of reaction rate expressions reported in the literature. Their recommendation, which will be followed in this paper, is to use the reaction rate expressions outlined by Achenbach and Riensche [19] as they are supposed to be typical of reformation reaction kinetics under SOFC anode conditions. The reaction rate expressions are shown below. Achenbach and Riensche recommend that

equation (4), for methane reformation, be governed by an Arrhenius rate expression as follows

$$R = \pm \nu k_0 P_{CH4} A \left(1 - \frac{Q}{K_{eq}}\right) e^{-E_a / R_u T} \quad (6)$$

Starting from left to right, R is the rate of reaction of equation (4); the sign of the equation is positive for the product species and negative for the reactant species; the coefficient v is the stoichiometric coefficient of the particular species; the pre-exponential factor k_0 is 4.274 kmol/(m^2-s-bar); the partial pressure of methane is P_{CH4} in bars; the surface area A of the node is known; the reaction quotient Q and equilibrium constant K_{eq} will be discussed in more detail later; the activation energy E_a is 82,000 kJ/kmol; the universal gas constant R_u is 8.314 kJ/(kmol-K); and the temperature of the node T is assumed to be the same as that at the exit of the node.

As shown in the following equations, the equilibrium constant can be found from the change in Gibbs free energy of the reaction Δg, and the reaction quotient is the product of the partial pressures of the products divided by the product of the partial pressures of the reactants, with the partial pressures being raised to their respective stoichiometric coefficients.

Since the water-gas shift reaction, equation (5), occurs very quickly, it is assumed that this reaction comes to equilibrium almost immediately. The reaction rate is thus expressed by the following equation.

$$R = \pm \nu k_0 A P_{CO} \left(1 - \frac{Q}{K_{eq}}\right) \quad (7)$$

The pre-exponential constant, A, in this case is just a sufficiently large number. The sign is positive for species being produced and negative for species being consumed. Also, note that the partial pressure of CO is used instead of the partial pressure of CH_4. Now in order to determine the temperature and species concentration gradients within the representative cell; the cell is discretized into a number of control volumes which will be discussed below.

Conservation of Mass

The two main sets of equations, conservation of mass and conservation of energy, are solved simultaneously in each of the nodes. It will be seen that the number of unknowns matches the number of equations so a unique solution is obtained. The conservation of mass is solved by the following equations for total number of moles:

$$\frac{dN}{dt} = \dot{N}_{in} + \sum R - \dot{N}_{out} \quad (8)$$

$$\dot{N}_{out} = \dot{N}_{in} + \sum R - \frac{d}{dt}\left(\frac{PV}{R_u T_{out}}\right) \quad (9)$$

Note that the amount of moles in the node is known through the ideal gas law. Also, in this discretized setup it is assumed that the mole fractions and temperature of the node are the same as those at the node exit. Of course, it would have been equally valid to use the mole fractions and temperature at the node inlet instead. Each of these assumptions produces an error, which can only be resolved by selection of an infinitesimally small node.

The conservation equations for the individual species can be found by expressing the moles of a species as the product of the total number of moles with the mole fraction of that species.

$$\frac{d}{dt}\left(N X_{out}\right) = \dot{N}_{in} X_{in} + R - \dot{N}_{out} X_{out} \quad (10)$$

$$X_{out} = \frac{R_u T_{out}}{PV} \int \left(\dot{N}_{in} X_{in} + R - \dot{N}_{out} X_{out}\right) dt \quad (11)$$

The value for the exit molar flow rate has not been explicitly solved for since it also appears in the integral on the right-hand side of the equation. But this is still acceptable since MATLAB Simulink® will be solving all of these equations simultaneously and dynamically. Note that the number of unknowns is two more than the number of equations so far, the extra unknowns being the exit temperature and the local current generation. So conservation of energy must be considered along with the Nernst equation and losses to garner a solution.

Conservation of Energy: Anode and Cathode Gases

There are four energy balances to consider for each node in the current model formulation. The energy balance of the anode gases, cathode gases, PEN, and plate. Careful bookkeeping is required to make sure that for each heat transfer mode associated with a given control volume there is heat transfer of equal magnitude associated with an adjacent control volume.

The anode gas and cathode gas energy balances simply state that the rate of change of internal energy at the node is equal to the rate of enthalpy in, plus the net enthalpy flux from the electrolyte, minus the rate of enthalpy out, plus the net heat flux in. Again, the temperature and mole fractions of the node are assumed to be the same as at the exit of the node.

$$\frac{dU}{dt} = \dot{H}_{in} + \dot{H}_{PEN} - \dot{H}_{out} + \sum \dot{Q} \quad (12)$$

$$U = \int \left(\dot{H}_{in} + \dot{H}_{PEN} - \dot{H}_{out} + \sum \dot{Q}\right) dt \quad (13)$$

$$U = \frac{PV}{R_u T_{out}} \sum X_{out} u(T_{out}) \quad (14)$$

For the anode, the net enthalpy flux from the electrolyte is affected by the H_2O entering and the H_2 leaving.

$$\dot{H}_{PEN} = R_{H2O} h_{H2O}(T_{PEN}) - R_{H2} h_{H2}(T_{out}) \quad (15)$$

For the cathode, the enthalpy flux is only affected by the O_2 leaving.

$$\dot{H}_{PEN} = -R_{O2} h_{O2}(T_{out}) \quad (16)$$

Now all that remains is to determine the heat fluxes. These fluxes are convective heat fluxes, where heat is transferred from the plate and also from the electrolyte.

$$\dot{Q}_{conv} = hA_i(T_i - T_{out}) \quad (17)$$

The above equation can represent the convection from the plate as well as the convection from the electrolyte by using the appropriate surface area, A_i, and temperature, T_i. The value of the convection coefficient is based upon the Nusselt number *Nu*. For the given geometry and flow rates, the value is 3.8 [22]. The convection coefficient can then be calculated using the following equation.

$$h = \frac{k}{D_c} Nu \quad (18)$$

The thermal conductivity of the fluid varies with temperature and although it cannot be known exactly without determining it empirically, it is estimated using the sum of the mole fractions times each of the constituent conductivities as follows

$$k = \sum X_i k_i(T_{out}) \quad (19)$$

This is a good first approximation. The values for the conductivities are interpolated or extrapolated from the tables found in [22]. The characteristic diameter D_c is the surface area exposed to the fluid divided by the wetted perimeter.

Conservation of Energy: PEN

The PEN temperature is found by performing another energy balance. The convection heat fluxes are taken to be positive when entering the gases or interconnect (see Figure 2).

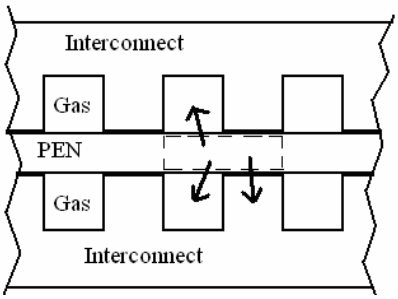

Figure 2. PEN energy balance.

As seen in Figure 2, there are three significant heat fluxes: convection from the anode gases, convection from the cathode gases, and conduction from the plate. The rate of conduction heat transfer from the PEN to the plate is expressed below.

$$\dot{Q}_{cond} = k_{int} A \frac{T_{PEN} - T_{int}}{L} \quad (20)$$

The area, *A*, is the contact surface area between the plate and the PEN, which is assumed to be half the area of that side of the control volume. But note that the two interconnects contact the PEN and exchgane heat with the PEN. The length, *L*, is half of the sum of the thickness of the interconnect and the PEN.

The rate of change of internal energy of the PEN equals the net heat flux minus the electric power produced. Also, the enthalpy of the H_2, O_2, and H_2O that entered the gas control volumes must be subtracted from this control volume in order to maintain conservation of energy as follows.

$$\frac{dU_{PEN}}{dt} = -\sum \dot{H}_{PEN} + \sum \dot{Q} - \dot{W}_{elec} \quad (21)$$

$$\sum \dot{Q} = -\dot{Q}_{conv,a} - \dot{Q}_{conv,c} - \dot{Q}_{cond} \quad (22)$$

$$T_{PEN} = \frac{1}{(\rho c V)_{PEN}} \int \left(-\sum \dot{H}_{PEN} + \sum \dot{Q} - IV\right) dt \quad (23)$$

Conservation of Energy: Interconnect

The energy balance for the interconnect is very similar to that of the PEN. Since many cells are stacked together, it is assumed that the representative cell being considered is well within the middle of the stack so that the control volume can be shifted to include half of the cell next to it, using a symmetry boundary condition. This way, the heat transfer from the anode and cathode gases can be considered using just one control volume.

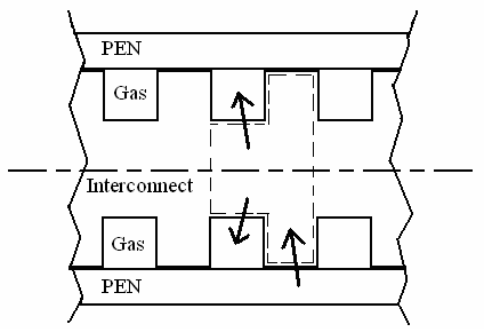

Figure 3. Interconnect energy balance.

Now to solve for the interconnect temperature, a simple energy balance is performed that only accounts for heat fluxes to and from adjacent control volumes.

$$\frac{dU_{\text{int}}}{dt} = \sum \dot{Q} \tag{24}$$

$$T_{\text{int}} = \frac{1}{(\rho c V)_{\text{int}}} \int \left(-\dot{Q}_{conv,a} - \dot{Q}_{conv,c} + \dot{Q}_{cond} \right) dt \tag{25}$$

The conduction heat transfer is the same as in the last subsection and the opposite sign has been accounted for in the above set of equations. The expressions for the convective heat transfer terms are the same as in a previous subsection except that the temperature of the interconnect is used in place of the PEN temperature and the surface area considered is half the area of the control volume plus the area of the two side walls which are related to the anode depth.

Nernst Equation

Finally, the current can be solved for using the famous Nernst equation with polarization loss terms as shown below.

$$V = E_0 - \frac{R_u T_{PEN}}{nF} \ln\left(\frac{P_{H2O}}{P_{H2} P_{O2}^{1/2}} \right) - \eta_{act} - \eta_{ohm} - \eta_{conc} \tag{26}$$

The value of n is two from the electrochemical half-reactions. The partial pressures are in bars. The ideal cell voltage E_0 is dependent on the change of Gibbs free energy of reaction which is a function of the temperature of the PEN.

$$E_0 = -\frac{\Delta g(T_{PEN})}{nF} \tag{27}$$

There are three polarization losses in equation (26), which are all functions of the local current generation. These polarizations are categorized as activation polarization, ohmic polarization, and concentration polarization.

The activation polarization is described by the following equation. As can be seen, the local current generation is compared to the exchange current density i_0 times the nodal PEN area.

$$\eta_{act} = \frac{2 R_u T_{PEN}}{nF} \sinh^{-1}\left(\frac{I}{2 j_0 A} \right) \tag{28}$$

The ohmic polarization is described by Ohm's Law. The resistance of the PEN is a function of temperature.

$$\eta_{ohm} = i R_{PEN}(T_{PEN}) \tag{29}$$

$$R_{PEN} = T_{PEN} \cdot e^{C1/T_{PEN} + C0} \tag{30}$$

Finally, the concentration polarization is described by the following equation.

$$\eta_{conc} = -\frac{R_u T_{PEN}}{nF} \ln\left(1 - \frac{I}{j_L A} \right) \tag{31}$$

In this case, the local current generation is compared to the limiting current density i_L times the nodal area of the PEN. The values used in the model for each of the parameters in these equations can be found in the Table 1 below.

TABLE 1. MODEL PARAMETERS

Parameter	Value	Units
Exchange Current Density	2000	A/m^2
Limiting current Density	9000	A/m^2
PEN thickness	0.5	mm
Interconnect thickness	2.5	mm
C1	7509.6	
C0	-25.855	
Cathode Channel Ht.	1.1	mm
Anode Channel Ht.	1.1	mm
PEN Density	5000	kg/m^3
PEN Specific Heat	0.8	kJ/kg-K
Plate Density	7900	kg/m^3
Plate Specific Heat	0.64	kJ/kg-K
Cell Width	10	cm
Cell Length	10	cm
Cell Active Area	100	cm^2

System Model

Hydrogen Collector

The hydrogen collector is only used for the case where the fuel cell is integrated into the system. It is approximated by simply removing 100% of the H_2 from the anode exhaust stream and it is assumed that the remaining mass is unaffected. An equilibrium calculation is performed after removal of the

hydrogen to accurately determine the remaining species compositions and temperature.

Combustor

The catalytic combustor works on a straightforward mass balance and then an energy balance. It is assumed that complete combustion can occur, then an equilibrium calculation proceeds to calculate the product species concentrations (CO_2, H_2O, CO, N_2, and O_2) and temperature.

Heat Exchanger

The heat exchangers are modeled in a counter-flow arrangement in which it is assumed that the efficiency is 90%. In other words, 10% of the heat transferred is lost to the environment. In addition, the heat exchange is limited by an approach temperature (pinch point) of 50 K (Note: In the model the approach temperatures were always greater than 75 K). The heat exchangers are modeled using the calorically-perfect gas assumption so that the amount of heat transferred is proportional to the log-mean temperature difference.

$$\Delta T_{lm} = \frac{\Delta T_1 - \Delta T_2}{\ln\left(\Delta T_1 / \Delta T_2\right)} \tag{32}$$

$$\Delta T_1 = T_{hot,in} - T_{cold,out} \tag{33}$$

$$\Delta T_2 = T_{hot,out} - T_{cold,in} \tag{34}$$

The log-mean temperature difference should always be positive since the local hot temperature is always greater than the local cold temperature. The heat transfer from the hot fluid to the cold fluid is determined from the following equations. The minus sign in the expression for hot fluid heat transfer indicates that the heat is leaving.

$$\dot{Q}_{hot} = -hA\Delta T_{lm} \tag{35}$$

$$\dot{Q}_{cold} = \varepsilon hA\Delta T_{lm} \tag{36}$$

The product of the effective convection coefficient and the surface area is chosen for each heat exchanger to give the desired inlet and exit temperatures at the calibrating conditions. A time delay is put into the heat exchangers so that the exit temperatures are determined by what the inlet temperatures were a few moments earlier. This delay is a rough approximation to the actual time it might take for the gas streams to flow through the heat exchangers, but more importantly it puts a break into the loop of equations being solved thereby making it easier for the model to converge because the set of equations is no longer elliptic.

Efficiencies

There are four efficiencies that are considered and reported in the results, which are electrical efficiency, H_2 production efficiency, electrochemical efficiency, and H_2 collection efficiency.

$$\varepsilon_{electric} = \frac{\dot{W}_{elec}}{\dot{N}_{CH4} M_{CH4} \left(LHV\right)_{CH4}} \times 100 \tag{37}$$

$$\varepsilon_{H2,production} = \frac{\dot{N}_{H2} M_{H2} \left(LHV\right)_{H2}}{\dot{N}_{CH4} M_{CH4} \left(LHV\right)_{CH4}} \times 100 \tag{38}$$

$$\varepsilon_{electrochem} = \frac{\dot{W}_{elec}}{\dot{N}_{CH4} M_{CH4} \left(LHV\right)_{CH4} - \dot{E}_{exh}} \times 100 \tag{39}$$

$$\varepsilon_{H2,collection} = \frac{\dot{N}_{H2} M_{H2} \left(LHV\right)_{H2}}{\dot{E}_{exhaust}} \times 100 \tag{40}$$

$$\dot{E}_{exhaust} = \dot{E}_{CH4,exh} + \dot{E}_{CO} + \dot{E}_{H2} \tag{41}$$

The energy rate in the denominator for the first two efficiencies is based on the lower heating value (LHV) of CH_4 in the inlet flow. For the electrical efficiency, the numerator contains the electrical power; and for the H_2 production efficiency, the numerator contains the chemical energy of the H_2 collected from the exhaust stream, again based on LHV. The electrochemical efficiency is similar to the electrical efficiency except that in the denominator the amount of chemical energy of the exhaust gases is subtracted from the chemical energy of the inlet fuel. And the H_2 collection efficiency is similar to the H_2 production efficiency except that the chemical energy of the exhaust gases is used in the denominator instead of the chemical energy of the inlet fuel.

ANALYSIS, RESULTS, AND DISCUSSION

Effect of "Extent of Pre-Reforming"

As was discussed in the introduction and background section, the fuel cell is integrated into a system where the fuel cell exhaust gases are catalytically combusted and used to preheat the inlet gases. In order to simplify the analysis for now, the fuel cell will be isolated from the rest of the system components and the inlet gas streams will be held at fixed temperatures of 1123 K. This set up is used to determine the effect of the extent of pre-reforming on the representative PEN temperature distribution in the stack for various operating conditions.

The stack is calibrated so that it will produce 1000 kW of power with the individual cells each having a voltage of 0.65 V at a fuel utilization of 85%, cathode exhaust temperature of 1273 K (1000 °C), and a SC ratio of three. These parameters

are similar to the ones chosen by Leal and Brouwer [23] in their thermodynamic analysis. It was determined that 35,800 cells are required to achieve the desired power output.

Three different cases of pre-reforming are considered. The first case is the one that is the main subject of this research where there is no pre-reforming and all the fuel is reformed internally. The second case is partial pre-reforming, and the third case is complete pre-reforming.

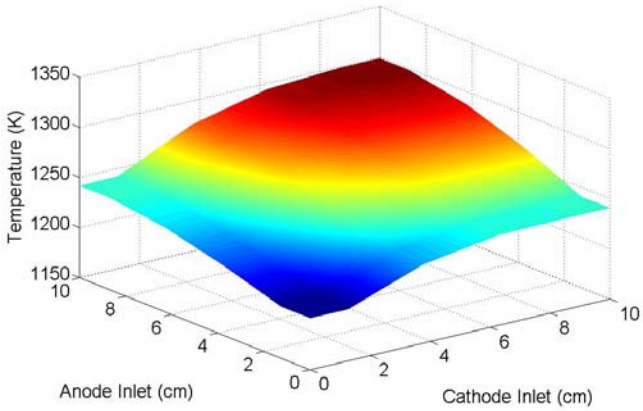

Figure 4. PEN temperature distribution for no pre-reforming at the calibrating conditions.

The temperature distribution of the fuel cell PEN for the case of no pre-reforming is shown in Figure 4. The position axes show the anode gases, which are fuel and steam, entering from the left and traveling to the right. The cathode gas, which is air, enters from the front and travels to the back. As can be seen, the maximum temperature differential is about 100 K. The perceived symmetry of the temperature distribution is only a coincidence.

Before showing the results of the partially and completely pre-reformed cases, a brief description will be given as to how partially and completely pre-reformed fuel is defined. Partially pre-reformed fuel is defined here as having anode species mole fractions that correspond to what they would be at equilibrium at 800 K. Similarly, completely pre-reformed fuel has anode species mole fractions that correspond to what they would be at equilibrium at 900 K. Note that the total number of moles of the anode stream must be scaled accordingly as it increases during the reformation process.

In all three cases the CH_4 flow rate is held constant at 37.62 g/s and the air flow rate is held constant at 526.45 g/s. The mole fractions of each species and the scaling factor for the total number of moles for the anode gases are shown in the following table.

TABLE 2. PRE-REFORMING CASES

Pre-reforming	CH_4	CO	CO_2	H_2	H_2O	Scaling Factor
None	.250	0	0	0	.750	1
Partial	.091	.017	.089	.405	.398	1.43
Complete	.025	.058	.092	.543	.282	1.49

Now the temperature distributions for partial and complete pre-reforming are shown in Figure 5.

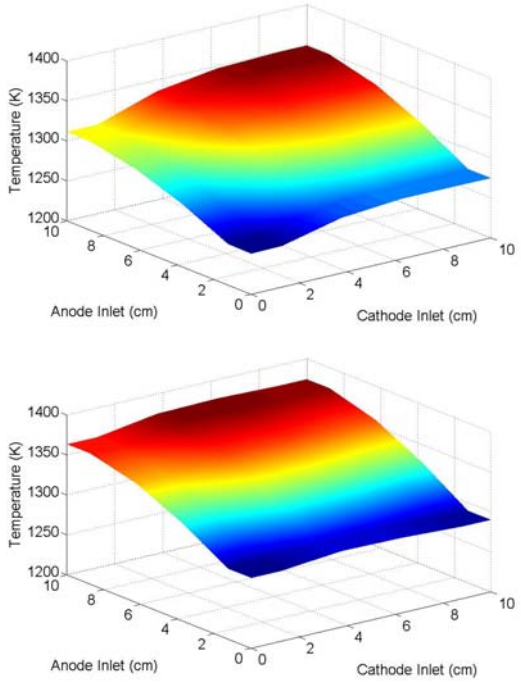

Figure 5. PEN temperature distribution for partial pre-reforming (TOP) and complete pre-reforming (bottom) at the calibrating conditions.

Note that the absolute temperatures of each distribution may be different, but the scaling is the same. The absolute temperature is not the focus right now since it could easily be changed by increasing the air flow rate and the number of cells in order to achieve the desired power. The focus in this subsection is on the temperature gradients across the cell, not the mean temperatures. From Figures 4 and 5 it can be seen that the maximum temperature differential is roughly 100 K for all three cases. This seems to suggest that the problem of large temperature gradients caused by internal reforming is not quite as daunting. In fact, from just the three graphs of temperature distributions so far, it would seem as if internal reforming actually evens out the temperature distribution better than partial and complete pre-reforming does.

Now in order to qualitatively interpret the graphs, first consider the case of complete pre-reforming. The endothermic reformation reactions are insignificant because almost all of the reforming was done before entering the fuel cell. So the two main thermal influences on the cell are the heat generated from

the exothermic electrochemical reactions and the convective cooling from the cathode flow. There is also convective cooling from the anode flow but it is not as significant because it travels at a much slower rate.

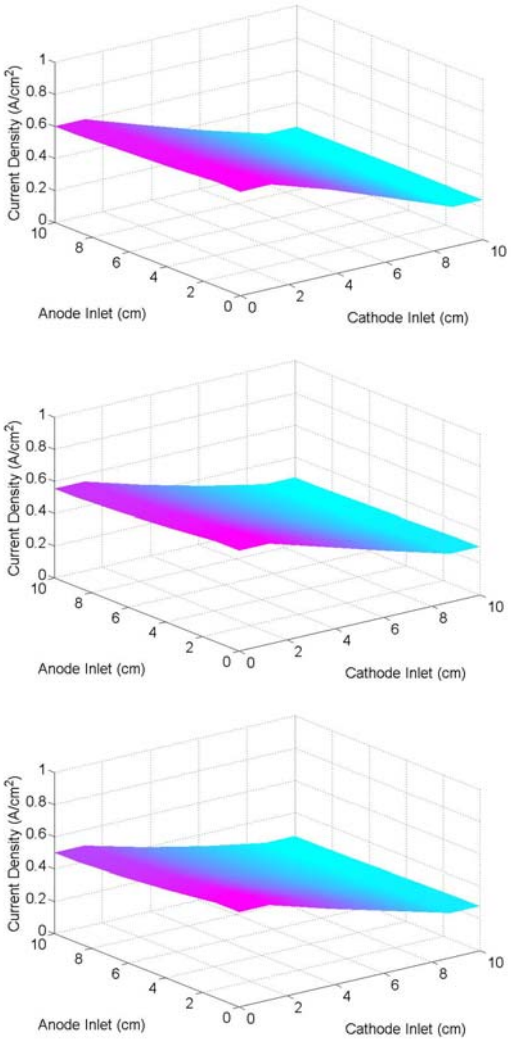

Figure 6. Current density distribution for no pre-reforming (top), partial pre-reforming (Middle), and complete pre-reforming (bottom) at the calibrating conditions.

As shown in Figure 6, the current density is highest near the anode inlet and decreases as the H_2 is depleted as it travels from the anode inlet to the anode exit. Since the electrochemical heat generation should correlate with the current density, it would be expected that absent the convective cooling the temperature should be greater near the anode inlet and lower near the anode exit. But that is not what is shown in Figure 5. This means that the convective cooling is the dominating thermal effect in this case. And as expected, the amount of heat transfer from convective cooling is large near the cathode inlet and decreases as the air flows through the cell because as the air absorbs the heat it becomes less effective at cooling the cell.

The endothermic reformation cooling effect for partial and no pre-reforming can be seen from the dips in the temperature distributions in Figures 4 and 5 near the anode inlet. But note that the temperature gradients caused by the internal reforming are not as large as the temperature gradients caused by the cathode flow convection.

Steady State System Analysis

Now the fuel cell is integrated into the rest of the system with the hydrogen collector, combustor, and heat exchangers. One difference between this analysis and the analysis in the previous subsection is that now the fuel cell inlet flow temperatures are dependent on the pre-heating from the exhaust stream. The hydrogen collector used in this setup collects all the H_2 from the exhaust stream and leaves all of the CO to be combusted. The purpose of doing this is to ensure that there is enough heat to preheat the inlet gas streams. The heat exchangers are sized so that the inlet temperatures are 1123 K at the calibrating conditions. The analysis consists of varying the fuel utilization and observing the steady state response of the system to these changes in fuel utilization. And just as before, the voltage and cathode exhaust temperature are held constant at 0.65 V and 1273 K, respectively.

From Figure 7 it can be seen how the fuel and air flow rates must be changed in order to keep the cathode exhaust temperature at 1273 K at different fuel utilizations. As expected, as the fuel utilization increases, the fuel flow rate must decrease.

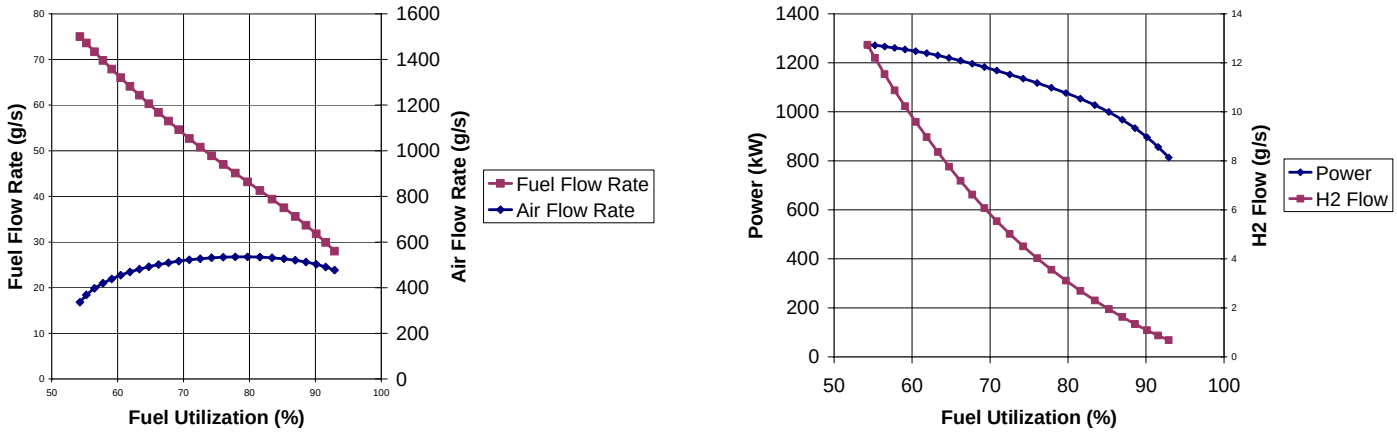

Figure 7. Variation of fuel and air flow rates with fuel utilization (left) and variation of power and H_2 production with fuel utilization (right) at constant cathode exhaust temperature of 1273 K.

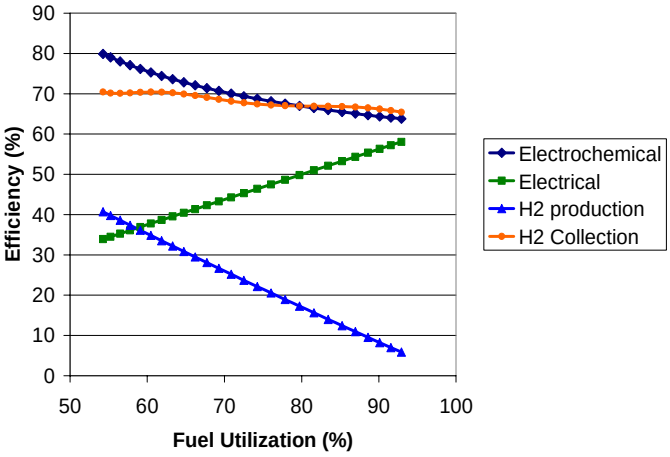

Figure 8. Variation of Electrical, H_2 production, electrochemical, and H_2 collection efficiencies with fuel utilization at constant cathode exhaust temperature of 1273 K.

And from Figure 7, since the air utilization decreases as the fuel utilization increases, the air flow rate must increase as well. This all agrees with intuition and shows that the model is working properly. Notice that the maximum power and maximum H_2 production both occur at low fuel utilizations. So there is no tradeoff between the two; either there is low power and low H_2 production, or high power and high H_2 production. Hence, the scenario of running the fuel cell at maximum power during the day and maximum H_2 production at night is unattainable.

Figure 8 shows the variation of the efficiencies with the fuel utilization. Note that the electrochemical efficiency reaches a maximum at the lower fuel utilizations. So it would seem that for a given cathode exhaust temperature, there is a quadruple benefit of running at low fuel utilization: there is maximum power, maximum H_2 production, maximum electrochemical efficiency, and minimum parasitic losses. However, one disadvantage of running at low fuel utilization is that the electrical efficiency is minimum, but this is just because the fuel is being converted to H_2 instead of electricity. Also, there is the possibility of large temperature gradients since the thermal effect of the endothermic fuel reformation will be greater and the thermal effect of the cathode convective cooling will be smaller because of the lower air flow rate.

The PEN temperature, CH_4 concentration, H_2 concentration, and current density distributions at a fuel utilization of 85% are shown in Figure 9. The PEN temperature and current density distributions are very similar to those shown in the previous subsection. Now these same distributions are explored for two other fuel utilizations, first at 70% then at 60%.

From Figure 10, notice that the maximum temperature differential has increased slightly to about 130 K. However, the dominant thermal influence is no longer the convective cooling from the cathode gases; but rather, it is the endothermic reformation cooling from the anode gases. It is also interesting to note that the current density is highest near the anode inlet. This suggests that near the anode inlet there is more heat generated from the electrochemical reactions than further downstream. However, the cooling from the reformation reactions clearly dominates over any temperature differential attempting to be established by the current density distribution. It is difficult to tell, however, how much of an effect the extra heat added by the electrochemical reactions near the anode inlet helps to smooth out the temperature gradient along the anode flow direction.

In Figure 11, now at an even lower fuel utilization of 60%, the reformation reactions clearly dominate the thermal influence over the cathode convective cooling. The maximum temperature differential has increased to about 150 K from the 130 K at 70% fuel utilization. Notice also that there is slightly less of a gradient in the current density distribution. This is most likely due to the smaller H_2 concentration gradient because less H_2 is being consumed in the cell.

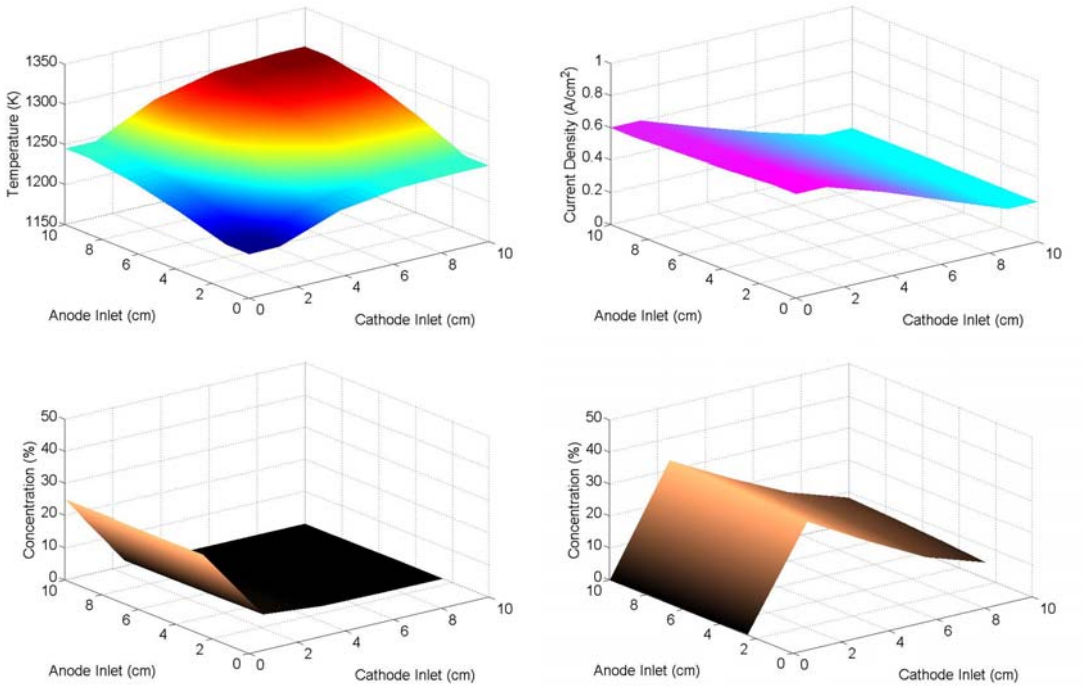

Figure 9. PEN temperature (top left), current density (top right), CH_4 concentration (bottom left), and H_2 concentration (bottom right) distributions at 85% fuel utilization and cathode exhaust temperature of 1273 K

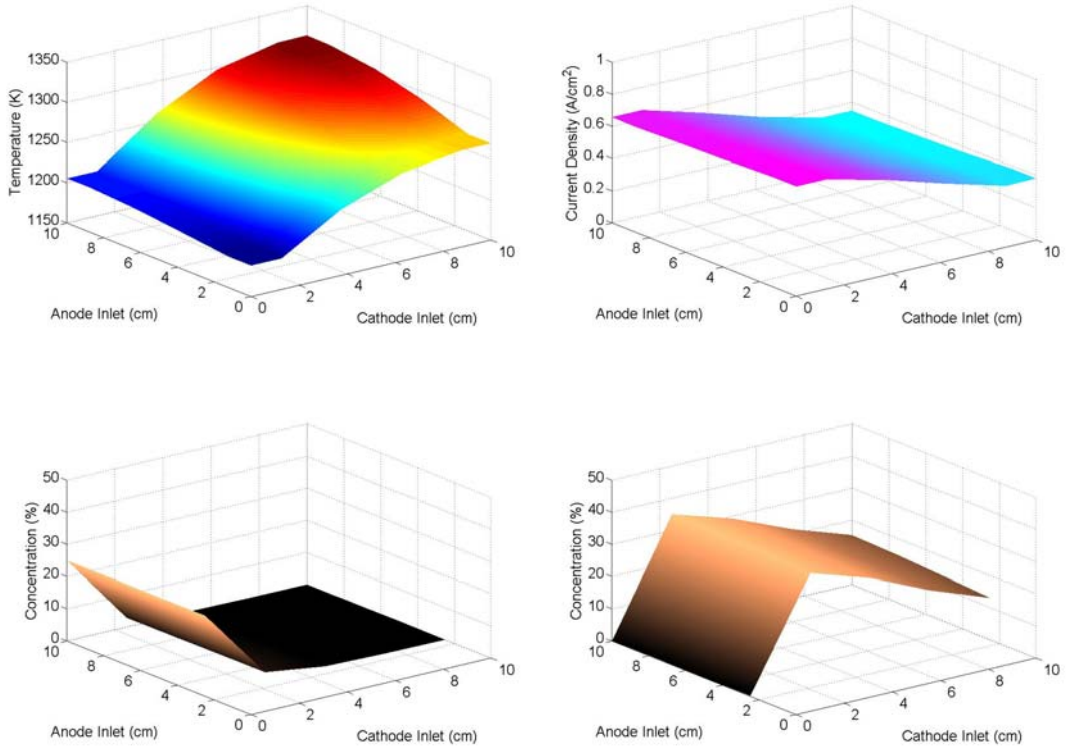

Figure 10. PEN temperature (top left), current density (top right), CH_4 concentration (bottom left), and H_2 concentration (bottom right) distributions at 70% fuel utilization and cathode exhaust temperature of 1273 K.

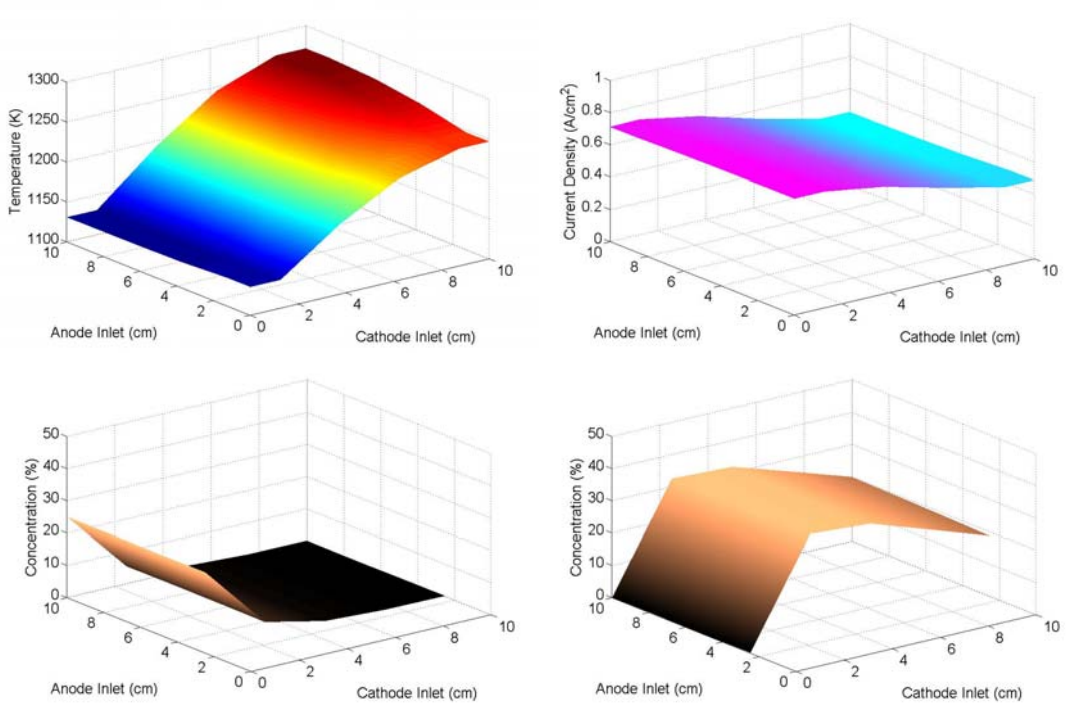

Figure 11. PEN temperature (top left), current density (top right), CH_4 concentration (bottom left), and H_2 concentration (bottom right) distributions at 60% fuel utilization and cathode exhaust temperature of 1273 K.

Dynamic Response

When this research was first started, the goal of this subsection was supposed to be to determine the dynamic response for switching between two different operating conditions while maintaining the same cathode exhaust temperature at the beginning and end of the process. One operating condition would give high power and low H_2 production while the other condition would give low power and high H_2 production. However, as was seen in the previous subsections, both high power and high H_2 production occurred at the same operating condition of low fuel utilizations, so it is not possible to try to switch from one to the other. So instead this section will present the dynamic response of an isolated fuel cell switching between a fuel utilization of 85% to 60%, while obtaining the same cathode exhaust temperature at the beginning and end of the process.

It can be seen from Figure 12 how the fuel and air flow rates are changed in a 5 minute time period. The rate at which the power and H_2 production change can be seen over a 10 minute time period. Notice how both the power and H_2 production reach steady-state almost by 5 minutes or a bit afterwards. Figure 12 shows how the H_2 production and power output of the stack can be controlled by changing the air and fuel flow rates. The figure also demonstrates how the model can be used for dynamic analyses as well.

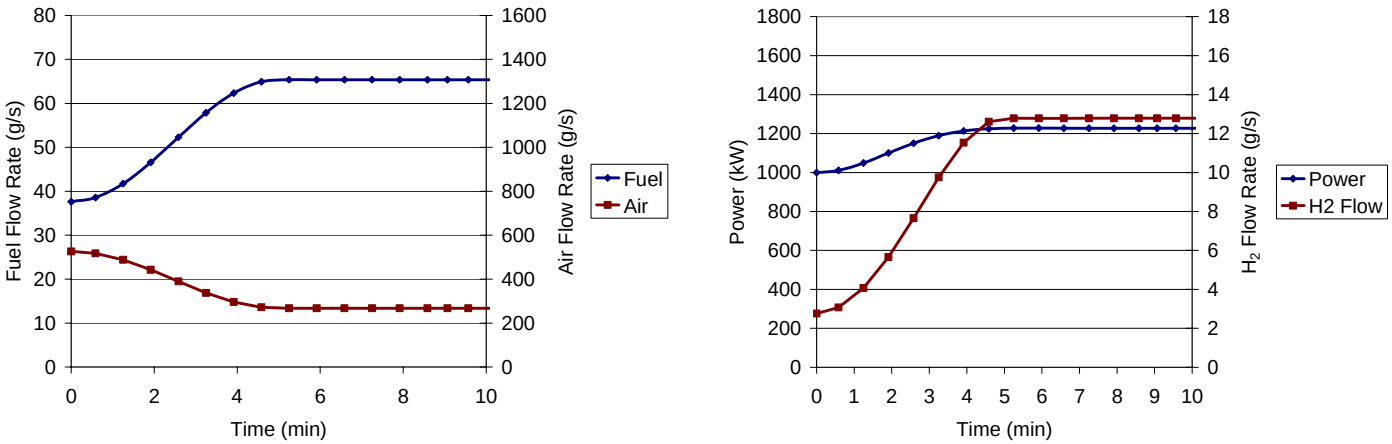

Figure 12. Fuel and air flow rates versus time (left) and power and H_2 production versus time (right) while switching from a fuel utilization of 85% to 60% and maintaining a cathode exhaust temperature of 1273 K at the beginning and ending conditions.

CONCLUSIONS

A quasi-3-dimensional model has been developed to study the dynamics of on-anode reforming of methane in a planar SOFC. The model has been applied to study of the impacts of varying fuel utilization during internal reforming for electricity and hydrogen co-production. The model shows the steady-state SOFC performance for various operating conditions and the dynamic response of the cell during fuel utilization transients. For each of the parametric variations and dynamic perturbations, the model was able to determine the two-dimensional PEN temperature, current density, CH_4 concentration, and H_2 concentration distributions. The main conclusions of this research are the following.

- Full internal reforming of methane, that is, with no pre-reforming, produced conditions with the highest across-cell temperature differentials compared to cases with partial or complete pre-reformation.

In all three cases investigated—no pre-reforming, partial pre-reforming, and complete pre-reforming—the maximum differential of the PEN temperature was roughly 150 K.

- For a given cathode exhaust temperature, the maximum power, the maximum H_2 production, the maximum electrochemical efficiency, and the minimum parasitic losses occur for conditions of lowest fuel utilization.

No tradeoff between power and H_2 production was found for a constant cathode exhaust temperature of 1273 K. Both high power output and high hydrogen co-production were realized for conditions of lowest fuel utilization studied (60%). The electrochemical efficiency increased as the power and H_2 production increased, and the air flow rate decreased resulting in lower blower parasitic losses.

- At low fuel utilizations, the endothermic reformation reactions are the primary contributors to the observed SOFC temperature profile.

- Maximum SOFC temperature differentials ranged from 150K for the 60% fuel utilization case to 100K for the 85% fuel utilization case.
- The quasi-3-D dynamic model was shown to be amenable to integration into a larger system model to predict both steady state performance and dynamic responses to fuel utilization perturbations.

The model considered in this paper is complex enough to resolve the dynamic physical and chemical processes in a quasi-3-D fashion while at the same time being simple enough to be used in a larger system simulation or to develop control strategies.

ACKNOWLEDGMENTS

We graciously acknowledge the financial support of the U.S. Department of Defense Fuel Cell Program of the Engineer Research and Development Center of the U.S. Army Corps of Engineers and our program manager, Mr. Franklin H. Holcomb.

NOMENCLATURE

A	Surface area: m^2
C	Specific heat: kJ/(kg-K)
D_c	Characteristic diameter: m
E_0	Ideal voltage: V
E_a	Activation energy: kJ/kmol
$\dot{E}$	Energy rate: kW
F	Faraday's constant: 96,485 kC/kmol
Δg	Change in Gibbs free energy of reaction: kJ/kmol
$\dot{H}$	Enthalpy rate: kW
H	Convection coefficient: kW/(m^2-K) or Specific enthalpy: kJ/kmol
i	Electrical current: kA
i_0	Exchange current density: kA/m^2
i_L	Limiting current density: kA/m^2
j	Current Density: kA/ m^2
L	Length: m
K	Thermal conductivity: kW/(m-K)
k_0	Pre-exponential constant: kmol/(m^2-s-bar)
K_{eq}	Equilibrium constant
M	Molar mass: kg/kmol
N	Mole number: kmol
$\dot{N}$	Molar flow rate: kmol/s
Nu	Nusselt number: (-)
N	Electron coefficient ratio: (-)
P	Pressure: kPa, bar
Q	Reaction quotient
$\dot{Q}$	Heat transfer rate: kW
R	Reaction rate: kmol/s or Resistance: Ω
R_u	Universal gas constant: 8.314 kJ/(kg-K)
T	Temperature: K
ΔT	Change in temperature: K
T	Time: s
U	Internal energy: kJ
U	Specific internal energy: kJ/kg
V	Voltage: V or Volume: m^3
$\dot{W}_{elec}$	Electrical power: kW
X	Species mole fraction: (-)
E	Efficiency: (-)
H	Polarization: V
P	Density: kg/m^3
N	Stochiometric coefficient: (-)

ACRONYMS

LHV	Lower Heating Value
SC	Steam-to-Carbon
PEN	Positive Electrode-Electrolyte-Negative Electrode
SOFC	Solid Oxide Fuel Cell

REFERENCES

[1] Brey, J. J., Brey, R., Carazo, A. F., Contreras, I., Hernández-Díaz, A. G., and Gallardo, V. "Designing a gradual transition to a hydrogen economy in Spain." Journal of Power Sources. Elsevier. 159 (2006) 1231-1240.

[2] Yuan, J. and Sundén, B. "Analysis of Chemically Reacting Transport Phenomena in an Anode Duct of Intermediate Temperature SOFCs." Journal of Fuel Cell Science and Technology. 3 (2006) 89-98.

[3] Dicks, A. L. "Hydrogen generation from natural gas for the fuel cell systems of tomorrow." Journal of Power Sources. Elsevier. 61 (1996) 113-124.

[4] Ming, Q., Healey, T., Allen, L., and Irving, P. "Steam reforming of hydrocarbon fuels." Catalysis Today. Elsevier. 77 (2002) 51-64.

[5] Sangtongkitcharoen W., Assabumrungrat, S., Pavarajarn V., Laosiripojana, N., and Praserthdam, P. "Comparison of carbon formation boundary in different modes of solid oxide fuel cells fueled by methane." Journal of Power Sources. Elsevier. 142 (2005) 75-80.

[6] Laosiripojana, N. and Assabumrungrat, S. "Catalytic steam reforming of methane, methanol, and ethanol over Ni/YSZ: The possible use of these fuels in internal reforming SOFC." Journal of Power Sources. Elsevier. 163 (2007) 943-951.

[7] Achenbach, E. (1994). "Three-dimensional and time-dependent simulation of a planar solid oxide fuel cell stack." Journal of power sources 49(1): 333.

[8] Kakac, S. (2007). "A review of numerical modeling of solid oxide fuel cells." International journal of hydrogen energy 32(7): 761-786.

[9] Aguiar, P., Adjiman, C. S., and Brandon, N. P. "Anode-supported intermediate temperature direct internal reforming solid oxide fuel cell. II: model-based Dynamic performance and Control." Journal of Power Sources. Elsevier. 147 (2005) 136-147.

[10] Qi, Y. (2005). "Dynamic modeling of solid oxide fuel cell: The effect of diffusion and inherent impedance." Journal of power sources 150(1): 32-47.
[11] Gemmen, R. S. and C. D. Johnson (2005). "Effect of load transients on SOFC operationâ€"current reversal on loss of load." Journal of Power Sources 144(1): 152-164.
[12] Qi, Y. (2006). "Dynamic modeling of a finite volume of solid oxide fuel cell: The effect of transport dynamics." Chemical engineering science 61(18): 6057-6076.
[13] Hall, D. J. (1999). "Transient modeling and simulation of a tubular solid oxide fuel cell." IEEE transactions on energy conversion 14(3): 749-753.
[14] Ota, T. (2003). "Object-based modeling of SOFC system: Dynamic behavior of micro-tube SOFC." Journal of power sources 118(1): 430-439.
[15] Xue, X. (2005). "Dynamic modeling of single tubular SOFC combining heat/mass transfer and electrochemical reaction effects." Journal of power sources 142(1): 211-222.
[16] Sedghisigarchi, K. (2004). "Dynamic and transient analysis of power distribution systems with fuel cells - Part I: Fuel-cell dynamic model." IEEE transactions on energy conversion 19(2): 423-428.
[17] Jiang, W. (2006). "Parameter setting and analysis of a dynamic tubular SOFC model." Journal of power sources 162(1): 316-326.
[18] Mueller, F., Brouwer, J., Jabbari, F., and Samuelsen, S. “Dynamic Simulation of an Integrated Solid Oxide Fuel Cell System Including Current-Based Fuel Flow Control.” Journal of Fuel Cell Science and Technology. 3 (2006) 144-154.
[19] Achenbach, E. and Riensche E. “Methane/steam reforming kinetics for solid oxide fuel cells.” Journal of Power Sources. Elsevier. 52 (1994) 283-288.
[20] Naterer, G. F. and Tokarz, C. D. “Entropy Based Design of Fuel Cells.” Journal of Fuel Cell Science and Technology. 3 (2006) 165-174.
[21] Aguiar, P., Adjiman, C. S., and Brandon, N. P. “Anode-supported intermediate temperature direct internal reforming solid oxide fuel cell. I: model-based steady-state performance.” Journal of Power Sources. Elsevier. 138 (2004) 120-136.
[22] Incropera, F. and DeWitt, D. Fundamentals of Heat and Mass Transfer. 5th ed. John Wiley & Sons, Inc.: Hoboken, NJ (2002).
[23] Leal, E. and Brouwer J. “A Thermodynamic Analysis of Electricity and Hydrogen Co-Production Using a Solid Oxide Fuel Cell.” Journal of Fuel Cell Science and Technology. 3 (2006) 137-143.